Universiteit Antwerpen

This item is the archived peer-reviewed author-version of:

3D culture of murine neural stem cells on decellularized mouse brain sections

Reference:

De Waele Jorrit, Reekmans Kristien, Daans Jasmijn, Goossens Herman, Berneman Zwi Nisan, Ponsaerts Peter.- *3D culture of murine neural stem cells on decellularized mouse brain sections*

Biomaterials - ISSN 0142-9612 - 41(2015), p. 122-131

DOI: http://dx.doi.org/doi:10.1016/j.biomaterials.2014.11.025

uantwerpen.be

Institutional repository IRUA

3D culture of murine neural stem cells on decellularized mouse brain sections

Jorrit De Waele[1,2], Kristien Reekmans[1,2], Jasmijn Daans[1,2], Herman Goossens[2], Zwi Berneman[1,2], Peter Ponsaerts[1,2]

[1] Experimental Cell Transplantation Group, Laboratory of Experimental Hematology, University of Antwerp, Antwerp, Belgium.

[2] Vaccine and Infectious Disease Institute (Vaxinfectio), University of Antwerp, Antwerp, Belgium.

Running title:

3D culture of neural stem cells

Corresponding author:

prof. dr. Peter Ponsaerts, Experimental Cell Transplantation Group, Laboratory of Experimental Hematology, Vaccine and Infectious Disease Institute (Vaxinfectio), University of Antwerp, Campus Drie Eiken (CDE-S6.51), Universiteitsplein 1, 2610 Antwerp (Wilrijk), Belgium.

Tel.: 0032-3-2652428 - E-mail: peter.ponsaerts@uantwerpen.be

Abstract

Transplantation of neural stem cells (NSC) in diseased or injured brain tissue is widely studied as a potential treatment for various neurological pathologies. However, effective cell replacement therapy relies on the intrinsic capacity of cellular grafts to overcome hypoxic and/or immunological barriers after transplantation. In this context, it is hypothesized that structural support for grafted NSC will be of utmost importance. With this study, we present a novel decellularization protocol for 1.5 mm thick mouse brain sections, resulting in the generation of acellular three-dimensional (3D) brain sections. Next, the obtained 3D brain sections were seeded with murine NSC expressing both the eGFP and luciferase reporter proteins (NSC-eGFP/Luc). Using real-time bioluminescence imaging, the survival and growth of seeded NSC-eGFP/Luc cells was longitudinally monitored for 1-7 weeks in culture, indicating the ability of the acellular brain sections to support sustained *ex vivo* growth of NSC. Next, the organization of a 3D maze-like cellular structure was examined using confocal microscopy. Moreover, under mitogenic stimuli (EGF and hFGF-2), most cells in this 3D culture retained their NSC phenotype. Concluding, we here present a novel protocol for decellularization of mouse brain sections, which subsequently support long-term 3D culture of undifferentiated NSC.

Keywords

brain, decellularization, growth scaffold, neural stem cells, bioluminescence imaging, 3D cell culture

Introduction

Due to their self-renewal capacity and their differentiation potential into neurons, astrocytes and oligodendrocytes [1], neural stem cells (NSC) are currently considered as ideal therapeutic candidates for the treatment of various neurodegenerative diseases and traumata to the central nervous system (CNS) [2]. Although most pre-clinical cell transplantation studies envisage grafting of single cell suspensions [3], it is not unlikely that the clinical success of NSC transplantation will be highly improved by the application of *in vitro* cultured 3D NSC structures [3, 4]. In this context, the traditional *ex vivo* culture of NSC in 3D aggregates, called neurospheres, has been at the forefront for many years. However, despite the fact that neurospheres are easily cultured *ex vivo*, it is generally accepted these *in vitro* NSC populations are not fully representative for the spatiotemporal behaviour of NSC *in vivo* [3]. The substantial heterogeneity that occurs during neurosphere expansion [5, 6], which in addition coincides with a high amount of apoptotic NSC/NPC within the core of neurospheres [5], are features rarely found in the *in vivo* 3D NSC niche [7]. Nevertheless, 3D culture of NSC offers many benefits, ranging from dynamic growth processes to the creation of gradients, which resemble the *in vivo* situation [6, 8, 9] and are crucial in many biological processes [9, 10].

Although recently a 3D cerebral organoid model derived from human pluripotent stem cells was developed [11], much attention has gone and still goes to NSC growth support using 3D bio-constructs. While support of NSC survival and growth has been demonstrated on 3D brain matrices developed from synthetic materials and/or purified biomaterials, including hydrogels [4, 12], synthetic polymers [13] and

designer self-assembling peptides [9, 14], it should be noted that these artificial growth scaffolds might contain uncontrollable toxic components [15] and - in simplified form - miss bioactivity [13] and cell adhesion molecules [4]. Furthermore, with the development of novel growth scaffolds for *ex vivo* cultured NSC, it should be recognized that the *in vivo* 3D NSC niche is highly complex and not yet fully understood [16]. In the NSC niche, not only the NSC themselves are of importance, but also the extracellular matrix (ECM) and supporting cells are important mediators in control of tissue maintenance and regeneration [3]. As the ECM comprises the secreted products of cells in a tissue, it therefore represents a potential suitable substrate for maintenance of a tissue-specific phenotype of a cell [17-19]. As such, attention has been given to the development of growth scaffolds containing whole ECM fractions or purified proteins thereof. An important feature of this approach is that such structures can function as a guiding structure during tissue regeneration [18] and/or release functional molecules during degradation [13].

Tissue decellularization is a methodology to remove cells from a specific tissue while preserving the ECM and its structural organisation. Most tissues are already subjected to decellularization processes, including - but not limited to - heart [20], lung [21] and kidney [22], and some have even already resulted into clinically approved medicinal products, such as pericardium and heart valves [23, 24]. However, going through recent literature, research on brain tissue decellularization [23] is limited due to: (i) the extreme fragility of brain tissue for decellularization procedures [24], and (ii) the more direct (commercial) application of other decellularized tissues, e.g. heart valves. Recently, two research groups employed different protocols to decellularize and solubilize porcine brain tissue, while

preserving bioactive ECM proteins [17, 24]. DeQuach et al. observed that solubilized brain matrix proteins can serve as coating material to support culture and maturation of neurons [24]. In addition, Crapo et al. demonstrated that addition of solubilized brain matrix to PC12 neuronal cultures resulted in longer neurite outgrowth and strongly altered cell migration and differentiation in comparison to the addition of matrix proteins derived from the urinary bladder, thereby confirming added value of tissue-specific ECM proteins during culture and differentiation [17, 25]. Furthermore, transplantation experiments reported by Bible et al. demonstrated the *in situ* viability of NSC in a hydrogel supplemented with porcine brain ECM [26]. Also Ribatti et al. demonstrated *in situ* that decellularized rat brain tissue induces a strong angiogenic response upon transplantation onto chick-embryo chorioallantoic membrane [27].

Up until now, brain tissue has rarely been decellularized with success and has, except for one study [27], always been solubilized for further use. However, acellular brain matrices carry the potential as ideal 3D *ex vivo* NSC culture system as they comprise the natural molecular and structural environment of brain cells and harbour necessary survival and differentiation signals [19, 28, 29]. Following our efforts to develop and validate a biological growth scaffold for NSC, we here present a novel decellularization protocol for mouse brain sections. Following seeding of NSC, viability and growth were validated using real-time bioluminescence imaging (BLI) and confocal microscopy. Moreover, post-fixation immunofluorescent stainings were applied to confirm NSC identity following 3D growth on the decellularized brain sections.

Materials and Methods

Decellularization of mouse brain sections

Wild-type C57BL/6 mice (n = 25) were obtained via Charles River Laboratories and further bred in the animal facility of the University of Antwerp until use for brain isolation (age of 2-4 months). Mice were kept in normal day-night cycle (12/12) with free access to food and water. For mouse brain isolation, mice were euthanized via an intra-peritoneal injection with 150 µl Nembutal (60 mg/ml, CEVA Sante Animale) followed by trans-cardiac perfusion with 0.9 % NaCl (Baxter, B1370). Subsequently, the brain was isolated, rinsed with phosphate-buffered saline (PBS, Gibco, 14200-067) and cut in 1.5 mm brain sections using a home-made razor blade device. The obtained brain sections (3-4/mouse brain) were then decellularized using the following protocol consisting out of three cycles employing demineralized water (dH_2O, Millipore RIOs), sodium deoxycholate (SDC, Sigma, 30970) diluted in dH_2O, DNase I (Sigma, D4263) diluted in 1 M NaCl solution (Fischer Scientific, S/3160/60) and Triton X-100 (TX-100, Sigma, X100) diluted in dH_2O. During the first decellularization cycle, brain sections placed in 24 well plates were subsequently incubated (each time in 1 ml) for 7 hours (h) in dH_2O, 14 h in 4 % SDC, 15 minutes (min) in PBS, 1 h in 40 kU/ml DNase, 15 min in PBS, 4 h in dH_2O, 2 h in 3 % Triton X-100, 15 min in PBS, 1 h in 40 kU/ml DNase and 15 min in PBS. The second and third cycle of decellularization consisted of 4 h in dH_2O, 12 h in 4 % SDC, 15 min in PBS, 1 h in 40 kU/ml DNase, 15 min in PBS, 2 h in dH_2O, 2 h in 3 % TX-100, 15 min in PBS, 1 h in 40 kU/ml DNase and 15 min in PBS. Finally, the brain sections were incubated in dH_2O for 1 h. All these steps were performed at 150 rpm in a KS 4000i control Incubator Shaker (IKA, Staufen, Germany) at room temperature (RT). All

solutions contained 200 U/ml penicillin (Invitrogen, 15140-122), 200 mg/ml streptomycine (Invitrogen, 15140-122) and 0.2 µg/ml amphotericin B (Invitrogen, 15290-018). In order to ensure removal of residual debris and to confirm sterility, the decellularized brain sections were incubated in neural expansion medium (NEM, see below for exact composition) for one week in a standard cell culture incubator at 37 °C, 5 % CO_2 and 80-90 % humidity. Photographs illustrating the decellularization procedure were taken using a Sony DSC-TX5 camera and are represented in Figure 1.

Microscopic validation of decellularized mouse brain sections

At first, evaluation of nuclear content removal was performed on whole decellularized brain sections. For this, decellularized and positive control non-decellularized brain sections were fixed for 1 h with 4 % paraformaldehyde (PFA, Sigma, 441244) and stained with 4',6-diamino-2-phenylindole (DAPI, 1 µg/ml, Sigma, D9564). The stained sections were visualized using a Nikon Eclipse Ti-E inverted microscope attached to a microlens-enhanced dual spinning disk confocal system (Ultra*VIEW* VoX; PerkinElmer, Zaventem, Belgium) equipped with 405 nm, 488 nm and 561 nm diode lasers for excitation of blue, green and red fluorophores, respectively. Images were acquired and processed using Volocity 6.0.1 software (Improvision, PerkinElmer). For further characterization, decellularized and positive control non-decellularized brain sections were fixed for 1 h with 4 % PFA, dehydrated in increasing sucrose (Sigma, S0389) gradient solutions (2 h in 5 % sucrose, 2 h in 10 % sucrose and overnight in 20 % sucrose) and snap-frozen in liquid nitrogen (Air Liquide, Herenthout, Belgium). Subsequently, 10 µm sections were cut using an HM500 cryomicrotome (Microm International, Walldorf, Germany) and collected on poly-L-lysine-coated (P8920,

Sigma) microscope glasses (Labonord). Standard haematoxylin-eosin (H&E, Haematoxylin & Eosin RAPID Stain Kit, Klinipath, 631210) staining was performed as follows: fixation in neutral buffered formalin, rinsing in tap water, 2 min Carrazi's haematoxylin, 20 sec wash in tap water, 20 sec eosin, rinsing in tap water, dehydration, clearing and mounting. Immunofluorescent staining for laminin was performed according to standard procedures. In brief, sections were washed in Tris-buffered saline solution (TBS), permeabilized with 0.1 % TX-100 for 30 min on a Stuart Mini Orbital Shaker SSM1 (Bibby Scientific, Staffordshire, UK) and incubated for 1 h in 20 % blocking serum in TBS. Next, the primary antibody rabbit anti-mouse laminin (1 µg/ml, Sigma, L9393) was added for overnight incubation at 4 °C in the dark. The following day, the sections were washed and subsequently incubated with the secondary antibody fluorescein isothiocyanate-conjugated goat anti-rabbit IgG (5 µg/ml, Jackson ImmunoResearch, 111-096-144) for 1 h at room temperature on a shaker. Finally, the stained sections were washed in TBS, counterstained with DAPI for 20 min, washed in dH_2O and mounted with Prolong Gold Antifade Reagent (Invitrogen, P36930). All images were taken using an Olympus BX51 standard research fluorescence microscope (Olympus, Aartselaar, Belgium) equipped with an Olympus DP71 digital camera. Olympus Cell^F Software was used for image acquisition and processing.

Molecular validation of decellularized mouse brain sections

DNA was isolated from non-decellularized control and decellularized brain sections using the Extract-N-Amp Tissue PCR Kit (Sigma, XNAT2) according to the manufacturer's instructions. Polymerase chain reaction (PCR) was carried out using the Extract-N-Amp PCR ReadyMix (Sigma, E3004) according to the manufacturer's

instructions using the following three primer pairs (Eurogentec, Seraing, Belgium): forward 5'-TGT-GTC-CGT-CGT-GGA-TCT-GA-3' and reverse 5'-TTG-CTG-TTG-AAG-TCG-CAG-GAG-3' for glyceraldehyde 3-phosphate dehydrogenase (GAPDH, 149-bp fragment), forward 5'-ACG-TAA-CAC-AGT-TCC-ACC-CG-3' and reverse 5'-CAT-GCT-TAA-CTC-TGC-AGG-CG-3' for β2-microglobulin (B2M, 178-bp fragment), and forward 5'-CCC-CAC-AAC-TCT-TCC-ATT-CT-3' and reverse 5'-GCA-GGA-GTG-ATA-GG-GGTC-AT-3' for TATA-binding protein (TBP, 102-bp fragment). The following PCR conditions were used: 3 min of initial denaturation at 94 °C followed by an experimentally determined number of amplification cycles (25 for GAPDH; 30 for B2M and TBP) consisting of denaturation for 30 seconds (sec) at 94 °C, annealing for 30 sec at 60 °C and elongation for 1 min at 72 °C, after which there was a final elongation step of 10 min at 72 °C prior to sample storage at 4 °C. The fragment length of the amplified PCR products was analysed by agarose gel (1 %) electrophoresis on a Consort EV231 device for 80 min at 200 V, 500 mA and 150 W. The PCR products were visualized using ultraviolet light in a Universal Hood Gel Imager (Bio-Rad, Temse, Belgium) with Quantity One 4.6.9 software (Bio-Rad). Real-time PCR was carried out using the same three primer pairs and using the *Power* SYBR Green PCR Master Mix (Applied Biosystems, 4367659) according to the manufacturer's instructions. The real-time PCR reaction was carried out in triplicate on a StepOne Plus Real-Time PCR System (Applied Biosystems, Gent, Belgium) using the following conditions: 10 min at 95 °C for AmpliTaq Gold enzyme activation, followed by 40 cycles consisting of denaturation for 15 sec at 95 °C and annealing/elongation for 1 min at 60 °C. StepOne v2.1 Software (Applied Biosystems) was used for data analysis.

2D NSC culture

A previously established enhanced green fluorescent protein (eGFP)-expressing NSC line derived from C57BL/6-eGFP transgenic mice (Jax Mice strain 003291) was cultured as described before [30, 31]. In brief, NSC were cultured on fibronectin-coated (5 µg/ml in PBS; R&D Systems, 1030-FN) T75 culture flasks (Greiner Bio-One, Wemmel, Belgium) in NEM consisting of Neurobasal-A Medium (Invitrogen, 10888-022) supplemented with 10 ng/ml epidermal growth factor (EGF, ImmunoTools, 11343407), 10 ng/ml human basic fibroblast growth factor (hFGF-2, ImmunoTools, 11343625), 100 U/ml penicillin, 100 mg/ml streptomycin, 0.5 µg/ml amphotericin B, 2mM L-glutamine (Invitrogen, 1074990), and 1 % modified N2 supplement. The modified N2 supplement consisted of Dulbecco's modified Eagle's medium (DMEM)/F12 (Gibco) supplemented with 7.5 mg/ml bovine serum albumin (BSA, Invitrogen, 15260-037), 2.5 mg/ml insulin (Sigma, I1882), 2 mg/ml apo-transferrin (Sigma, T1147), 0.518 µg/ml sodium selenite (Sigma, S5261), 1.6 mg/ml putrescine (Sigma, P5780), and 2 µg/ml progesterone (Sigma, P8783). NSC cultures were incubated at 37 °C, 5 % CO_2 and 80-90 % humidity. For routine cell culture, NEM was replaced each 3-4 days and NSC cultures were split 1:5 every 7-8 days following harvesting using Accutase (Sigma, A6964) treatment. Routine assessment of eGFP expression and cell viability was performed on an Epics XL-MCL analytic flow cytometer (Beckman Coulter, Suarlée, Belgium) after addition of GelRed (1:1000, Biotum) for live/dead cell discrimination. Flow cytometric data were analysed using FlowJo Software (Tree Star Inc, Ashland, Oregon USA). In order to allow for real-time bioimaging of NSC growth, the eGFP-expressing NSC were additionally transduced with a lentiviral vector (LVv) encoding the luciferase (Luc) reporter protein (kindly provided by the Leuven viral vector core, Molmed, KULeuven, Belgium). For

LVv transduction, NSC-eGFP were cultured in fibronectin-coated 24-well plates until 70 % confluence. Next, medium (750 µl NEM) was refreshed and 10 µl of the LVv stock ($3.1x10^7$ pg/ml p24) was added to the NSC culture. 24 hours after transduction, medium was replaced with fresh NEM and transduced cells were selected by adding 10 µg/ml puromycin (Invivogen, ant-pr) to the medium. Following selection of transduced cells, NSC-eGFP/Luc were further cultured in NEM as described above and used throughout this study. For immunophenotyping experiments, NSC-eGFP/Luc were grown on fibronectin-coated glass coverslips (Marienfeld-Superior, 01 115 20) in 24-well plates. For *in vitro* differentiation of NSC-eGFP/Luc, cells were cultured on fibronectin-coated cover slips for three days in 1 ml neural differentiation medium, consisting of Neurobasal-A Medium supplemented with NeuroCult Neural Stem Cell Differentiation Supplements (StemCell Technologies, 05703), according to the manufacturer's instructions.

Immunofluorescence analysis of 2D NSC cultures

Immunocytochemical phenotyping of NSC-eGFP/Luc and *in vitro* differentiated NSC-eGFP/Luc in monolayer 2D cultures was performed using the following primary antibodies (Supplementary Table S1): rabbit anti-mouse sex determining region Y box 2 (SOX2, 1 µg/ml, CHEMICON, AB5603), rabbit anti-mouse brain lipid binding protein (BLBP, 0.5 µg/ml, CHEMICON, AB9558), rabbit anti-mouse Ki67 (5 µg/ml, Abcam, ab15580), rabbit anti-mouse glial fibrillary acidic protein (GFAP, 4.5 µg/ml, Abcam, ab7779), rabbit anti-mouse S100 calcium binding protein β (S100β, 1 µg/ml, Abcam, ab52642), mouse IgG2a anti-mouse neuronal class III β-tubulin (TuJ1, 4 µg/ml, R&D Systems, MAB1195). These primary antibodies were combined with the following fluorophore-conjugated secondary antibodies: Alexa Fluor 555 (AF555)-

conjugated donkey anti-rabbit IgG (2 µg/ml, Invitrogen, A31572) or AF555-conjugated goat anti-mouse IgG (10 µg/ml, Invitrogen, A21425). Note that different fixation and permeabilization protocols were used dependent on the target protein. For staining of 2D NSC-eGFP/Luc and *in vitro* differentiated 2D NSC-eGFP/Luc cultures, cells (on coverslips) were fixed for 1 h at RT with 4 % PFA for cytoplasmatic staining or at 4 °C with BD Cytofix/Cytoperm (BD, 554714) for nuclear staining. Next, the staining was performed as described above under the section microscopic validation of decellularized mouse brain sections, with following adjustments, (i) PBS was used for washing steps, (ii) solutions containing 10 % milk powder were changed to 0.1 % BSA, and (iii) for staining of nuclear proteins, 0.1 % TX-100 was added during blocking and antibody incubation steps to ensure nuclear permeabilization.

3D NSC culture

Two seeding procedures were evaluated to initiate NSC culture on the obtained decellularized mouse brain sections. At first, an injection-based approach was followed. For this, obtained brain sections were placed in a 24-well plate in 100 µl NEM supplemented with a ten-fold concentration of growth factors (10X GF, i.e. 100 ng/ml EGF and hFGF-2). Next, harvested NSC-eGFP/Luc were injected directly in the brain sections at a concentration of 6,7 x 10^5 cells (in 5 µl NEM + 10X GF) using a 10 µl Hamilton syringe with 30-gauge needle (Hamilton, Bonaduz, Switzerland) coupled to an automatic micro-injector pump (kdScientific, Holliston, Massachusetts, USA) in a stereotactic frame. Following three injections, cell-seeded brain sections were incubated for 1 h at 37 °C before fresh NEM + 10X GF was added up to a volume of 1 ml. In a second seeding approach, NSC were allowed to spontaneously adhere to and grow on the decellularized brain sections. For this, 2 x 10^6 NSC-

eGFP/Luc were added to a well containing the brain section in 1 ml NEM with 10X GF on day 0. For both culture strategies, every following 1-2 days the medium was changed with NEM + 2.5X GF (i.e. 25 ng/ml EGF and hFGF-2) to clear the cultures from freely growing neurospheres and to support 3D growth on/in the decellularized brain sections.

Bioluminescence imaging

For BLI of control cell cultures, harvested NSC-eGFP/Luc were seeded in black 96-well plates (Elscolab, Kruibeke, Belgium) at a concentration of 1 x 10^5 cells/well in 100 µl NEM. Immediately after administration of D-luciferin (5 µl of 30 mg/ml stock concentration in PBS, Promega, E1605), plates were imaged for 5 min using a real-time Biospace Photon Imager system (Biospace Lab, Paris, France). For BLI of NSC-eGFP/Luc cultures on decellularized brain sections, 50 µl D-luciferine was added to the culture wells. After 15 min of pre-incubation, the wells were imaged for 5 min using a real-time Biospace Photon Imager system. Light emission was detected by a charge-coupled device and at the end of the acquisition a photographic image of the plate was obtained. The data were quantified and analysed using M3 Vision software (Biospace Lab). Light emission from a fixed region of interest was measured. Values of signal intensity are presented as the average number of photons per second per square centimetre per steradian (ph/s/cm^2/str) during a 5-min time period.

Immunofluorescence analysis of 3D NSC cultures

Analysis of cellular viability of 3D NSC-eGFP/Luc cultures was carried out via direct eGFP fluorescence and by DAPI staining on cultures for live cell imaging. To study dimensionality, some 3D brain sections were cut in 100-150 µm slices using a

HM650V vibratome (Microm International, Walldorf, Germany) with cooled tissue bath (4 °C) prior to DAPI staining. Images were taken using a Nikon Eclipse Ti-E inverted microscope attached to a microlens-enhanced dual spinning disk confocal system (Ultra*VIEW* VoX). Images were acquired and processed using Volocity 6.0.1 software. For immunophenotyping, the 3D NSC-eGFP/Luc cultures were fixed for 1 h at RT with 4 % PFA for cytoplasmatic staining or at 4 °C with BD Cytofix/Cytoperm for nuclear staining. Next, the above-described procedures for microscopic validation of decellularized mouse brain sections were used with minor adjustments, (i) permeabilization was done with 0.1 % TX-100 for cytoplasmatic staining and 1 % TX-100 for nuclear staining, (ii) permeabilization time was increased to 2 h, (iii) TX-100 was also added during all antibody incubation steps (0.1 % TX-100 was added for cytoplasmatic staining and 1 % TX-100 for nuclear staining), (iv) incubation with the secondary antibody was carried out for 4 h, and (vi) no mounting medium was used as stained 3D cultures were directly imaged using the above-described inverted microscopy setup. The same antibodies and concentrations were used as described above for immunophenotyping of (differentiated) 2D NSC cultures.

Statistical analysis

Statistical analysis was performed on real-time PCR and immuncytochemical data. Real-time PCR data were tested for normality using Kolmogorov-Smirnov. Results derived from different number of decellularization cycles were statistically compared using the Kruskal-Wallis test with Bonferroni correction on the p-value. Quantification numbers from immunocytochemistry data were statistically compared using the Mann Whitney U-test. Tests were performed using GraphPad Prism 5.0 (San Diego, California, USA).

Results

Generation of decellularized mouse brain sections

We first developed a decellularization procedure for 1.5 mm mouse brain sections. The followed procedure, which consists of a pre-treatment procedure, the actual decellularization procedure and a post-treatment procedure, is briefly summarized in Figure 1 and described in detail in the Materials and Methods section. From the representative images provided, it can be clearly noted that decellularized brain sections become morphologically smaller, thinner, whiter and more transparent during the whole decellularization procedure (Figure 1B). Further direct confocal microscopy analysis on a decellularized mouse brain section revealed the absence of $DAPI^+$ nuclei (Figure 2A, lower panel), as compared to the clear presence of $DAPI^+$ nuclei in fresh non-decellularized mouse brain sections (Figure 2A, upper panel). In addition, PCR- and real-time PCR-based analysis for detection of a 178-bp β2-microglobulin (B2M) DNA fragment confirmed, respectively, the absence of a B2M PCR product after gel electrophoresis (Figure 2B) and significantly ($p < 0.0001$) higher C_t-values (Figure 2C) when performing the reactions on genomic DNA samples isolated from decellularized mouse brain sections that completed the three decellularization cycles, as compared to partially or non-decellularized mouse brain sections. Similar results were obtained following PCR- and real-time PCR-based analysis for detection of a 149-bp glyceraldehyde 3-phosphate dehydrogenase (GAPDH) and a 102-bp TATA-binding protein (TBP) DNA fragment (data not shown). Further characterisation of the obtained decellularized mouse brain sections included standard H&E staining and immunofluorescent staining for laminin in combination with nuclear DAPI staining on 10 µm cryosections obtained from decellularized 1.5

mm mouse brain sections (respectively Figure 2D and 2E). In comparison with the same staining procedure on 10 µm cryosections obtained from non-decellularized brain sections, the absence of nuclei can be clearly observed in decellularized brain sections, while - at least in part - protein content seems to be spatially preserved. These results indicate that the proposed decellularization procedure for 1.5 mm brain sections is able to efficiently elicit removal of nuclear material, while at the same time preserving tissue architecture and proteins of the decellularized mouse brain sections.

3D culture of mouse neural stem cells on decellularized mouse brain sections

In order to real-time visualize growth of seeded NSC on decellularized mouse brain sections, we took advantage of the functional properties of both the eGFP and luciferase reporter proteins. For this, we used a previously established and characterized eGFP-expressing NSC line derived from transgenic C57BL/6-eGFP mice [30] and further engineered this NSC-eGFP line using a lentiviral vector encoding the luciferase reporter protein, as described in the Materials and Methods section. The resulting NSC-eGFP/Luc line displayed high level of eGFP fluorescence, as demonstrated by direct fluorescence microscopy and flow cytometry analysis (Figure 3A), and high luciferase activity, as demonstrated by *in vitro* BLI analysis (Figure 3B). In a first experimental approach, NSC-eGFP/Luc were seeded into decellularized brain sections via three independent injections at distinct locations. Next, growth of seeded NSC-eGFP/Luc was monitored by real-time BLI. As shown in Figure 4A, dynamically growing NSC-eGFP/Luc cultures, as evidenced by spatiotemporal changes in the intensity and localization of the detected photon emissions, were obtained over a period of 1-7 weeks. Further quantitative analysis of

the obtained BLI signals during a two-week monitoring period indicated eight cultures to display increasing BLI signals, while the total luciferase activity remained stable over time in three other cultures and was decreased in one culture (Figure 4B, left graph). In addition, three cultures were further monitored up to seven weeks post-seeding. While two cultures displayed an increasing photon emission over time, the third culture remained stable over time (Figure 4B, right graph). Finally, as our BLI data already indicate a highly dynamic growth pattern of NSC on decellularized mouse brain sections, we further investigated the origin of the observed BLI signals by live cell imaging. The presence of viable cells growing in 3D in/on decellularized brain sections was confirmed by the direct detection of eGFP-expressing cells both in the XY plane (top-down view, Figure 4C, left image) and in the Z plane (coronal section, Figure 4C, middle image) of NSC-eGFP/Luc growing on a decellularized brain section. Note that cells in the obtained 3D cultures are organized in a maze-like structure (Figure 4C, right image). Furthermore, the combination of BLI with direct confocal microscopy allows for dual confirmation of long-term 3D NSC culture on decellularized mouse brain sections (Figure 4D).

Characterization of 3D NSC cultures on decellularized mouse brain sections

In this part of our study we aimed to further characterize the obtained 3D NSC cultures by means of immunofluorescence analysis. First, in order to demonstrate the NSC character of our 2D NSC cultures, we performed antibody staining against the following proteins: SOX2, BLBP, Ki67, TuJ1, S100β and GFAP. As shown by the representative images provided in Figure 5 (2D NSC), the phenotype of 2D NSC cultures can be characterized as $SOX2^+$ $BLBP^+$, without noticeable expression of the differentiation markers TuJ1, S100β and GFAP. A vast majority of the NSC in 2D

culture also express the proliferation marker Ki67 (56 % ± 3 %, n = 1). In agreement with our previous studies [11], 2D NSC cultures can readily be induced to differentiate along the astroglial and neuronal lineage, as demonstrated by the appearance of respectively S100β$^+$ GFAP$^+$ astrocytes and TuJ1$^+$ developing neurons (Figure 5, 2D NSC DIFF). The same phenotypic characterization was then performed on 3D NSC cultures. In agreement with our observations on 2D NSC cultures, 3D NSC cultures can be characterized as SOX2$^+$ BLBP$^+$ (Figure 5, 3D NSC). While no spontaneous differentiation into TuJ1$^+$ neurons was detected, a small amount of cells displayed expression of the S100β, but not GFAP, astrocyte marker. More remarkably, as compared to 2D NSC cultures, expression of the proliferation marker Ki67 was significantly ($p < 0.05$) reduced in 3D cultures (11 % ± 4 %, n = 3). Serial confocal Z-axis images for the different phenotypic characterisation stainings on the obtained 3D NSC cultures are provided in Supplementary Figure S1. These results suggest that the majority of cells in the 3D NSC cultures maintained their NSC phenotype and are not differentiated towards astrocytes or neurons, despite a reduction in proliferation potential. However, it should be noted here that, despite the fact that NSC can develop into expanding 3D cultures upon injection into decellularized mouse brain sections, the overall viability of these cultures is rather limited. As such, based on the number of DAPI$^+$ eGFP$^+$ nuclei versus the total number of DAPI$^+$ nuclei, the percentage of viable cells within these 3D NSC cultures was estimated 8.0 % ± 0.2 % (n = 3).

Improved viability of 3D NSC cultures

As limited intrinsic viability of 3D NSC cultures might hamper their further study, in a second experimental approach we aimed to improve overall viability of the 3D NSC

cultures by allowing seeded NSC to adhere and grow spontaneously onto decellularized mouse brain sections (n = 6). As shown in Figure 6A, longitudinal (up to 5 weeks) BLI monitoring of these samples confirmed that NSC seeded onto decellularized mouse brain sections generate viable and expanding 3D NSC cultures. Further microscopy analysis revealed (Figure 6B and Supplementary Figure S2), based on the number of $DAPI^+$ $eGFP^+$ nuclei versus the total number of $DAPI^+$ nuclei, a significantly ($p < 0.05$) increased percentage of viable cells within these spontaneously developing 3D NSC cultures (57 % ± 18 %, n = 4), as compared to the developing 3D NSC cultures following injection into the decellularized mouse brain sections.

Discussion

In this study we present a novel decellularization procedure for 1.5 mm mouse brain sections, which results in the generation of an acellular ECM / tissue protein scaffold able to support long-term growth of undifferentiated NSC. Although not described in detail in the results section of this manuscript, several technical issues needed attention during experimental progress in this study. Firstly, due to the intrinsic fragility of brain sections [24], which further increased during the decellularization procedure, it is recommended to apply very slow pipetting when changing solutions following the first SDC incubation in order to avoid destruction of the brain tissue sections. This fragility issue was also of importance for the generation of cryosections in order to characterize the obtained scaffold and/or seeded NSC populations. However, in our experimental setup we were obliged to use a cryosectioning approach as paraffin-embedding interferes with the detection eGFP-expressing NSC by direct fluorescence microscopy. For these reasons, most of the characterisation studies were performed using confocal microscopy on whole 3D ECM or cell-seeded ECM structures. Nevertheless, respresentative cryosections were obtained and stained to demonstrate the absence of nuclear content, with – at least in part – the preservation of protein content (eosin and laminin staining) and tissue architecture. Further studies will now have to reveal the complex nature of many different proteins still present in the obtained decellularized brain tissue scaffolds. Secondly, the proposed post-treatment procedure, whereby decellularized brain tissue sections are incubated for one week at 37°C in cell culture medium is highly recommended to remove residual cellular debris and/or remnants of potential cytotoxic components (i.e. SDC and TX-100). As such, we were only successful in obtaining viable 3D NSC

cultures when applying this post-treatment procedure to decellularized brain tissue sections. Without this procedure, injected NSC populations underwent rapid (within days) cell death and no expanding 3D NSC cultures could be obtained (data not shown). In course of our results we cannot exclude that similar cell death - albeit to a lower extent – lies at the basis of the low viability of the obtained 3D NSC cultures when injecting NSC directly into the obtained brain tissue scaffolds. However, the issue of low viability was solved when allowing seeded NSC to develop themselves onto the obtained brain tissue scaffolds. Currently, we have to leave open the question whether or not the obtained 3N NSC cultures develop themselves in or – by support of – on the brain tissue sections. To investigate the latter, we will need to develop an approach whereby ECM protein from the original brain tissue matrix can be distinguished from newly ECM matrix proteins produced by the 3D NSC culture.

By combining multimodal imaging techniques, i.e. BLI and direct confocal microscopy, the development of 3D NSC cultures on decellularized brain tissue sections can be non-invasively demonstrated over time. This is an important technical advantage when monitoring 3D tissue growth, which – following the approach presented in this manuscript – will certainly be further improved over the next years. Non-invasive imaging techniques will also allow for selection of high quality 3D NSC cultures for further experimental (or in time clinical) purpose. This selection procedure might become important, as – in contrast to artificial synthetic or biological scaffolds – the use of decellularized brain sections is associated with a lower experimental control over scaffold structure, as both intra-brain and inter-brain variations might occur in terms of decellularization outcome. Nevertheless, in comparison to spontaneously developing neurospheres, where only 0.1 - 0.2 %

would be true NSC [32], growth of NSC on decellularized brain tissue sections, albeit under stimulation of EGF and FGF, can maintain a generally undifferentiated NSC culture. Furthermore, we believe a mean viability of 57% for our 3D NSC cultures on decellularized brain tissue sections to be highly acceptable in comparison to the use of alternative biological 3D matrices. In most studies, biomaterial matrices for 3D NSC modelling are generally used as hydrogels. Viability of NSC in collagen hydrogels ranges from 61 - 84 %, dependent on the type of NSC (embryonic, postnatal, adult) and the addition of ECM components (hyaluronan) [33, 34]. In contrast however, Koutsopoulos and Zhang observed a decreased viability upon long-term culture of NSC in collagen hydrogels, i.e. from 55 % to only 25 % [15]. A similar but less profound effect was observed following NSC culture in Matrigel scaffolds (37 % viability) [15]. Of note, NSC viability in Matrigel peaks in the first two weeks, likely due to growth factors and cytokines intrinsically present in the Matrigel [15]. Popular alternative hydrogels are based on $RADA_{16}$ SAP, often loaded with functional motifs. Viability of NSC is generally sustained in such hydrogels [35], and was found to be higher (46 - 69 %) than collagen hydrogels or Matrigel in a comparative study [15]. Scaffolds based on synthetic polymers have also been used for 3D culture of NSC, e.g. using graphene foam or polyglycolic acid, and generally render a very high NSC viability (90 % and 99 %, respectively) [36, 37].

With our specific interest in cell and/or tissue transplantation research, we realize that general viability of our 3D NSC constructs still needs to be improved in order to limit endogenous immune response triggered by apoptotic and necrotic cells [6, 38]. One such approach would be the manipulation of scaffold porosity via perforation in order to increase diffusion of oxygen/nutrients to the core of the decellularized brain tissue

sections and to allow for improved cellular distribution [39]. However, perforation might also destroy tissue architecture, which is an important asset of decellularized tissues. Alternatively, co-development of blood vessel structures within 3D neural cell cultures might improve diffusion and growth pattern. Linke et al. seeded endothelial cells onto a decellularized scaffold prior to addition of hepatocytes in order to obtain a 3D vascularized liver tissue [40]. The preservation of vascular structures in the decellularized tissue allowed the endothelial cells to develop into a primitive vascular endothelium [40]. The retention of laminin, also present in normal vascular basement membrane [41], in our decellularized mouse brain sections renders pre-vascularization an intriguing future option. In addition, one might also aim to improve removal of dead cellular material. While in NSC monocultures death cells are removed by spontaneous release, in 3D cultures this is at least partially impeded as death cell material remains trapped in the cell mass. Hence, clearance of death cell material will aid overall viability. As such, addition of isogenic microglial cell populations, either primary or differentiated from embryonic stem cells [42], might be beneficial to further increase the overall viability within these 3D cultures due to their intrinsic phagocytic properties to clear apoptotic and necrotic cell material [43].

Finally, as this study demonstrates the possibility to initiate and to non-invasively monitor the growth of undifferentiated 3D NSC cultures by means of BLI and validated by confocal microscopy, further studies will now have to address the 3D differentiation potential of these 3D NSC cultures into complex networks of neurons, astrocytes and oligodendrocytes. Given the complexity of these assays, they were not the primary aim of this study, but are of specific interest within our future research goals. In view of embryonic brain development, such differentiation strategies might

require sequential seeding of different neural progenitor cell populations and/or growth factor support [44]. Nevertheless, given the experimental ease by which 3D NSC cultures spontaneously develop onto decellularized brain sections, it would be highly interesting to evaluate co-seeding of multiple (differentiated) cell populations, even from different lineages. Furthermore, in view of transplantation purposes, grafting of 3D tissue cultures might provide a solution for anoikis, besides lack of oxygen/nutrient support, a major issue leading to death of grafted cell population in the CNS [45, 46]. Although grafted 3D tissue cultures consisting out of multiple brain cell populations might capture growth and/or differentiation and/or survival factors from the brain milieu, it remains to be established whether such structures are able to survive on their own by supporting neo-angiogenesis or whether novel strategies need to be developed for the co-development of blood vessel structures within 3D neural cell cultures, as suggested above. Clearly, before such applications can arise experimentally (for drug testing) and clinically (for transplantation purposes), many more fundamental cell and developmental biology questions need to be unravelled and applied to 3D neural tissue culture models.

Conclusions

In this study we provided a first step in the development of undifferentiated 3D NSC cultures using decellularized mouse brain sections as growth scaffolds and validated our approach using non-invasive bioluminescence imaging and non-invasive / post-fixation confocal microscopy. Although many further developments are still necessary, we believe our approach - as it is for the moment - already to become useful for new research on the development of neural networks, brain tumour remodelling, drug testing and brain cell transplantation research.

Acknowledgements

This work was supported by research grants G.0136.11, G.0131.11 and G.0130.11 (granted to Zwi Berneman and Peter Ponsaerts) of the Fund for Scientific Research-Flanders (FWO-Vlaanderen, Belgium) and in part by a Methusalem research grant from the Flemish government (granted to Herman Goossens). We acknowledge helpful assistance from the BioImaging Laboratory at the University of Antwerp (Annemie Van der Linden) for support with bioluminescence imaging. We also acknowledge helpful technical support from the Biomedical Microscopic Imaging service facility at the University of Antwerp (Isabel Pintelon) for image analysis of 3D NSC cultures.

References

[1] Temple S. The development of neural stem cells. Nature 2001;414:112-7.

[2] Reekmans K, Praet J, De Vocht N, Daans J, Van der Linden A, Berneman Z, et al. Stem cell therapy for multiple sclerosis: preclinical evidence beyond all doubt? Regen Med 2012;7:245-59.

[3] Reekmans K, Praet J, Daans J, Reumers V, Pauwels P, Van der Linden A, et al. Current challenges for the advancement of neural stem cell biology and transplantation research. Stem Cell Rev 2012;8:262-78.

[4] Ma W, Fitzgerald W, Liu QY, O'Shaughnessy TJ, Maric D, Lin HJ, et al. CNS stem and progenitor cell differentiation into functional neuronal circuits in three-dimensional collagen gels. Exp Neurol 2004;190:276-88.

[5] Meletis K, Wirta V, Hede SM, Nister M, Lundeberg J, Frisen J. p53 suppresses the self-renewal of adult neural stem cells. Development 2006;133:363-9.

[6] Reekmans K, De Vocht N, Praet J, Fransen E, Le Blon D, Hoornaert C, et al. Spatiotemporal evolution of early innate immune responses triggered by neural stem cell grafting. Stem Cell Res Ther 2012;3:56.

[7] Biebl M, Cooper CM, Winkler J, Kuhn HG. Analysis of neurogenesis and programmed cell death reveals a self-renewing capacity in the adult rat brain. Neurosci Lett 2000;291:17-20.

[8] Kim H, Cooke MJ, Shoichet MS. Creating permissive microenvironments for stem cell transplantation into the central nervous system. Trends Biotechnol 2012;30:55-63.

[9] Zhang S, Gelain F, Zhao X. Designer self-assembling peptide nanofiber scaffolds for 3D tissue cell cultures. Semin Cancer Biol 2005;15:413-20.

[10] Baker BM, Chen CS. Deconstructing the third dimension: how 3D culture microenvironments alter cellular cues. J Cell Sci 2012;125:3015-24.

[11] Lancaster MA, Renner M, Martin CA, Wenzel D, Bicknell LS, Hurles ME, et al. Cerebral organoids model human brain development and microcephaly. Nature 2013;501:373-9.

[12] Wolf MT, Daly KA, Brennan-Pierce EP, Johnson SA, Carruthers CA, D'Amore A, et al. A hydrogel derived from decellularized dermal extracellular matrix. Biomaterials 2012;33:7028-38.

[13] Badylak SF, Freytes DO, Gilbert TW. Extracellular matrix as a biological scaffold material: Structure and function. Acta Biomater 2009;5:1-13.

[14] Santos E, Hernandez RM, Pedraz JL, Orive G. Novel advances in the design of three-dimensional bio-scaffolds to control cell fate: translation from 2D to 3D. Trends Biotechnol 2012;30:331-41.

[15] Koutsopoulos S, Zhang S. Long-term three-dimensional neural tissue cultures in functionalized self-assembling peptide hydrogels, matrigel and collagen I. Acta Biomater 2013;9:5162-9.

[16] Lutolf MP, Gilbert PM, Blau HM. Designing materials to direct stem-cell fate. Nature 2009;462:433-41.

[17] Crapo PM, Medberry CJ, Reing JE, Tottey S, van der Merwe Y, Jones KE, et al. Biologic scaffolds composed of central nervous system extracellular matrix. Biomaterials 2012;33:3539-47.

[18] Narayanan K, Leck KJ, Gao S, Wan AC. Three-dimensional reconstituted extracellular matrix scaffolds for tissue engineering. Biomaterials 2009;30:4309-17.

[19] Zhang Y, He Y, Bharadwaj S, Hammam N, Carnagey K, Myers R, et al. Tissue-specific extracellular matrix coatings for the promotion of cell proliferation and maintenance of cell phenotype. Biomaterials 2009;30:4021-8.

[20] Ott HC, Matthiesen TS, Goh SK, Black LD, Kren SM, Netoff TI, et al. Perfusion-decellularized matrix: using nature's platform to engineer a bioartificial heart. Nat Med 2008;14:213-21.

[21] Ott HC, Clippinger B, Conrad C, Schuetz C, Pomerantseva I, Ikonomou L, et al. Regeneration and orthotopic transplantation of a bioartificial lung. Nat Med 2010;16:927-33.

[22] Song JJ, Guyette JP, Gilpin SE, Gonzalez G, Vacanti JP, Ott HC. Regeneration and experimental orthotopic transplantation of a bioengineered kidney. Nat Med 2013;19:646-51.

[23] Crapo PM, Gilbert TW, Badylak SF. An overview of tissue and whole organ decellularization processes. Biomaterials 2011;32:3233-43.

[24] DeQuach JA, Yuan SH, Goldstein LS, Christman KL. Decellularized porcine brain matrix for cell culture and tissue engineering scaffolds. Tissue Eng Part A 2011;17:2583-92.

[25] Medberry CJ, Crapo PM, Siu BF, Carruthers CA, Wolf MT, Nagarkar SP, et al. Hydrogels derived from central nervous system extracellular matrix. Biomaterials 2013;34:1033-40.

[26] Bible E, Dell'Acqua F, Solanky B, Balducci A, Crapo PM, Badylak SF, et al. Non-invasive imaging of transplanted human neural stem cells and ECM scaffold

remodeling in the stroke-damaged rat brain by (19)F- and diffusion-MRI. Biomaterials 2012;33:2858-71.

[27] Ribatti D, Conconi MT, Nico B, Baiguera S, Corsi P, Parnigotto PP, et al. Angiogenic response induced by acellular brain scaffolds grafted onto the chick embryo chorioallantoic membrane. Brain Res 2003;989:9-15.

[28] Aumailley M, Gayraud B. Structure and biological activity of the extracellular matrix. J Mol Med (Berl) 1998;76:253-65.

[29] Singelyn JM, DeQuach JA, Seif-Naraghi SB, Littlefield RB, Schup-Magoffin PJ, Christman KL. Naturally derived myocardial matrix as an injectable scaffold for cardiac tissue engineering. Biomaterials 2009;30:5409-16.

[30] Praet J, Reekmans K, Lin D, De Vocht N, Bergwerf I, Tambuyzer B, et al. Cell type-associated differences in migration, survival, and immunogenicity following grafting in CNS tissue. Cell Transplant 2012;21:1867-81.

[31] Reekmans K, De Vocht N, Praet J, Le Blon D, Hoornaert C, Daans J, et al. Quantitative evaluation of stem cell grafting in the central nervous system of mice by in vivo bioluminescence imaging and postmortem multicolor histological analysis. Methods Mol Biol 2013;1052:125-41.

[32] Reynolds BA, Rietze RL. Neural stem cells and neurospheres--re-evaluating the relationship. Nat Methods 2005;2:333-6.

[33] Brannvall K, Bergman K, Wallenquist U, Svahn S, Bowden T, Hilborn J, et al. Enhanced neuronal differentiation in a three-dimensional collagen-hyaluronan matrix. J Neurosci Res 2007;85:2138-46.

[34] Ge D, Song K, Guan S, Qi Y, Guan B, Li W, et al. Culture and differentiation of rat neural stem/progenitor cells in a three-dimensional collagen scaffold. Appl Biochem Biotechnol 2013;170:406-19.

[35] Cheng TY, Chen MH, Chang WH, Huang MY, Wang TW. Neural stem cells encapsulated in a functionalized self-assembling peptide hydrogel for brain tissue engineering. Biomaterials 2013;34:2005-16.

[36] Li N, Zhang Q, Gao S, Song Q, Huang R, Wang L, et al. Three-dimensional graphene foam as a biocompatible and conductive scaffold for neural stem cells. Sci Rep 2013;3:1604.

[37] Park KI, Teng YD, Snyder EY. The injured brain interacts reciprocally with neural stem cells supported by scaffolds to reconstitute lost tissue. Nat Biotechnol 2002;20:1111-7.

[38] Praet J, Santermans E, Daans J, Le Blon D, Hoornaert C, Goossens H, et al. Early inflammatory responses following cell grafting in the CNS trigger activation of the sub-ventricular zone: a proposed model of sequential cellular events. Cell Transplant 2014.

[39] Bergmeister H, Boeck P, Kasimir MT, Fleck T, Fitzal F, Husinsky W, et al. Effect of laser perforation on the remodeling of acellular matrix grafts. J Biomed Mater Res B Appl Biomater 2005;74:495-503.

[40] Linke K, Schanz J, Hansmann J, Walles T, Brunner H, Mertsching H. Engineered liver-like tissue on a capillarized matrix for applied research. Tissue Eng 2007;13:2699-707.

[41] Nikolova G, Jabs N, Konstantinova I, Domogatskaya A, Tryggvason K, Sorokin L, et al. The vascular basement membrane: a niche for insulin gene expression and Beta cell proliferation. Dev Cell 2006;10:397-405.

[42] Beutner C, Roy K, Linnartz B, Napoli I, Neumann H. Generation of microglial cells from mouse embryonic stem cells. Nat Protoc 2010;5:1481-94.

[43] Tambuyzer BR, Ponsaerts P, Nouwen EJ. Microglia: gatekeepers of central nervous system immunology. J Leukoc Biol 2009;85:352-70.

[44] Barberi T, Klivenyi P, Calingasan NY, Lee H, Kawamata H, Loonam K, et al. Neural subtype specification of fertilization and nuclear transfer embryonic stem cells and application in parkinsonian mice. Nat Biotechnol 2003;21:1200-7.

[45] Radakovits R, Barros CS, Belvindrah R, Patton B, Muller U. Regulation of radial glial survival by signals from the meninges. J Neurosci 2009;29:7694-705.

[46] Ruoslahti E, Reed JC. Anchorage dependence, integrins, and apoptosis. Cell 1994;77:477-8.

Figure legends

Figure 1. Visual representation of the developed decellularization prodecure.

(A) Brain pre-treatment prior to decellularization to obtain 1.5 mm mouse brain sections. (B) Decellularization procedure. Images are representative for shape, size and colour of the 1.5 mm mouse brain section during the whole decellularization procedure. (C) Post-treatment of decellularized mouse brain sections. A step-by-step protocol description is provided in the Materials and Methods section. dH_2O: demineralised water; SDC: sodium deoxycholate; TX-100: Triton X-100.

Figure 2. Microscopic and molecular validation of decellularized mouse brain sections.

(A) Representative direct confocal image obtained from a DAPI-stained decellularized 1.5 mm mouse brain section (lower image, 3c: 3 decellularisation cycles, n = 1 brain tissue analysed) demonstrating the absence of $DAPI^+$ nuclei in contrast to the provided representative direct confocal image from a control non-decellularized 1.5 mm mouse brain section (upper image, PC: positive control, n = 1 brain tissues analysed). Note that the high DAPI background in the decellularized mouse brain section is due to increased light exposure time in order to visualize the scaffold structure. (B) Agarose gel electrophoresis reveals absence of 178-bp β2-microglobulin (B2M) PCR fragments in genomic DNA isolated from decellularized mouse brain sections (1.5c, 1.5 decellularisation cycle, n = 1; 3c, 3 decellularization cycles, n = 5) in contrast to control non-decellularized mouse brain sections (PC, positive control, n = 2). NC: no template water control (n = 1). (C) Real-time PCR analysis confirms absence of 178-bp B2M PCR fragments in genomic DNA isolated

from samples subjected to the full decellularization protocol (3c, n = 5), while only minute amounts are detectable in brain sections subjected to half the decellularization procedure (1.5c, n = 1). The 178-bp B2M PCR fragment is readily detected in control non-decellularized mouse brain sections (PC, positive control, n = 2). Data are presented as mean +/- standard deviation (n = 6 for each condition). (D) Representative haematoxylin-eosin (H&E) staining on 10 µm cryosections obtained from a decellularized and a non-decellularized 1.5 mm mouse brain section (for each, n = 1 brain tissue analysed). (E) Representative laminin / DAPI staining on 10 µm cryosections obtained from a decellularized and a non-decellularized 1.5 mm mouse brain section (for each, n = 1 brain tissue analysed).

Figure 3. Reporter protein expression by C57BL/6 NSC-eGFP/Luc.

(A) NSC-eGFP/Luc display high level of eGFP fluorescence as measured by direct fluorescence microscopy and by flow cytometric analysis (inset). Representative images were chosen from, respectively, 52 and 12 independent analyses. (B) *In vitro* BLI confirms high luciferase activity as measured by light emission by NSC-eGFP/Luc upon addition of the luciferin substrate. Data are presented as mean +/- standard deviation (n = 8). BLI: bioluminescence imaging; eGFP: enhanced green fluorescent protein; Luc: luciferase; NSC: neural stem cell.

Figure 4. Growth properties of NSC-eGFP/Luc seeded in decellularized mouse brain sections.

(A) Spatiotemporal changes in intensity and localization of detected photon emission demonstrate a dynamic growth pattern of NSC-eGFP/Luc on decellularized mouse brain sections during a seven-week monitoring period. The provided images

correspond to quantitative data shown by the upper line in the right image of panel B below. (B) Relative growth properties of NSC-eGFP/Luc on decellularized mouse brain sections during a 2-week (n = 12) and 7-week (n = 3) monitoring period. The dashed line indicates the initial BLI signal at day 1 post-seeding. For graphical representation data were normalized (i.e. BLI signal on day 1 was set to a value of 1). (C) Direct detection of $eGFP^+$ cells by confocal microscopy in the XY (left image) and Z plane (middle image) demonstrating a 3D growth pattern of NSC-eGFP/Luc on decellularized mouse brain sections. Representative images were chosen from 25 analyses. A detailed view from Z-stacked XY planes indicates that these 3D cultures are organised in a maze-like structure (right panel). (D) Representative examples providing confocal microscopy of 3D NSC cultures with the corresponding BLI analysis (n = 2 for day 3, n = 4 for days 7 and 14, and n = 5 for day 5). 3D: three-dimensional; BLI: bioluminescence imaging; eGFP: enhanced green fluorescent protein; NSC: neural stem cell.

Figure 5. Phenotypic analysis of 2D and 3D NSC cultures.

NSC in 2D culture (left column, 2D NSC), NSC differentiated in 2D culture (middle column, 2D NSC DIFF) and NSC in 3D culture (3D NSC) were analysed by immunocytochemical staining for neural stem cell markers (BLBP and SOX2), the proliferation marker Ki67, the neuronal differentiation marker TuJ1, the astrocyte differentiation markers S100β and GFAP, and the intrinsic viability marker eGFP. DAPI staining was used to visualize the nuclei. Representative images were chosen from at least 2-3 different stainings per condition analysed. 2/3D: two-/three-dimensional; BLBP: brain lipid binding protein; DAPI: 4',6-diamino-2-phenylindole; eGFP: enhanced green fluorescent protein; GFAP: glial fibrillary acidic protein; NSC:

neural stem cell; S100β: S100 calcium binding protein β; SOX2: sex determining region Y box 2; TuJ1: neuronal class III β-tubulin.

Figure 6. Growth properties of NSC-eGFP/Luc seeded on decellularized mouse brain sections.

(A) Absolute growth properties of NSC-eGFP/Luc on decellularized mouse brain sections during a 5-week period (n = 6). (B) Direct detection of $DAPI^+$ $eGFP^+$ cells by confocal microscopy in the XY plane on decellularized mouse brain sections. A representative image was chosen from 10 analyses. 3D: three-dimensional; BLI: bioluminescence imaging; DAPI: 4',6-diamino-2-phenylindole; eGFP: enhanced green fluorescent protein; NSC: neural stem cell.

Supplementary Figure legends

Figure S1. Serial confocal Z-axis images for the different phenotypic characterisation stainings on the obtained 3D NSC cultures.

Serial confocal Z-axis images for the images from 3D NSC cultures presented in Figure 5. Interval measure is shown in brackets. 3D: three-dimensional; BLBP: brain lipid binding protein; DAPI: 4',6-diamino-2-phenylindole; eGFP: enhanced green fluorescent protein; GFAP: glial fibrillary acidic protein; NSC: neural stem cell; S100β: S100 calcium binding protein β; SOX2: sex determining region Y box 2; TuJ1: neuronal class III β-tubulin.

Figure S2. Serial confocal Z-axis images of 3D NSC cultures

Serial confocal Z-axis images (6 μm interval) for the image presented in Figure 6C. DAPI: 4',6-diamino-2-phenylindole; eGFP: enhanced green fluorescent protein.

FIGURE 1

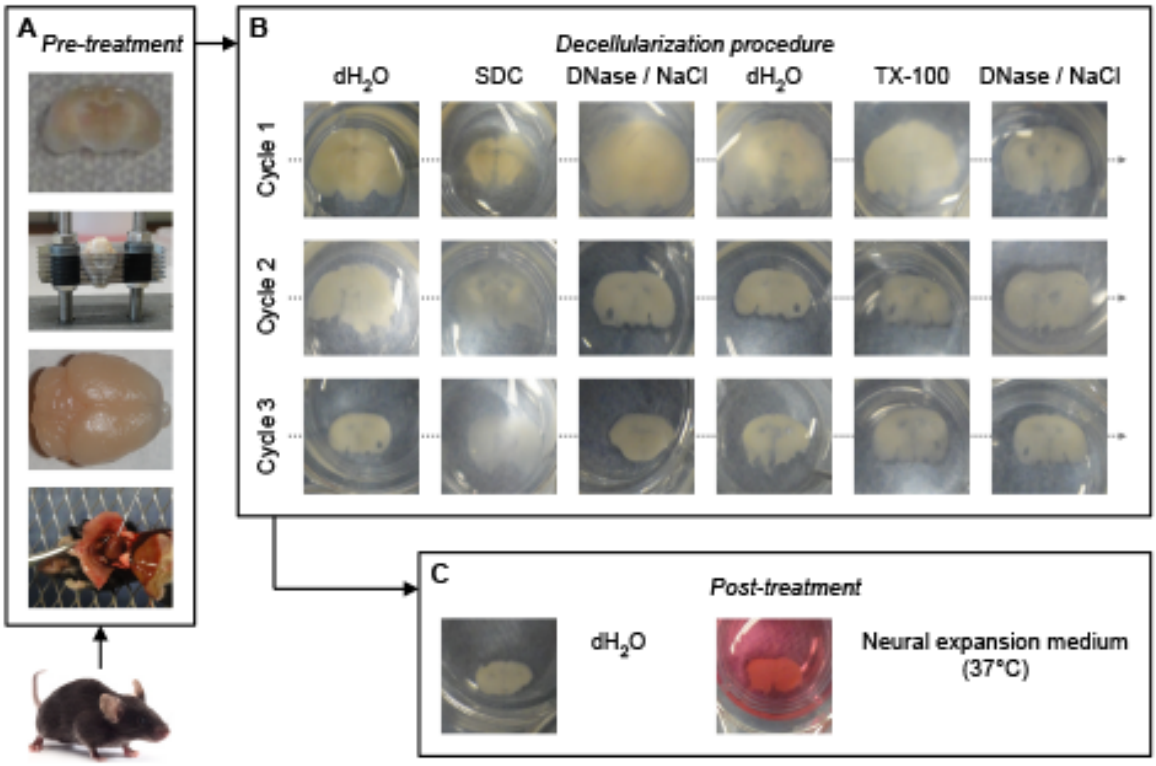
A
Pre-treatment
B
Decellularization procedure
dH2O
SDC
DNase / NaCl
dH2O
TX-100
DNase / NaCl
Cycle 1
Cycle 2
Cycle 3
C
Post-treatment
dH2O
Neural expansion medium
(37°C)

FIGURE 2

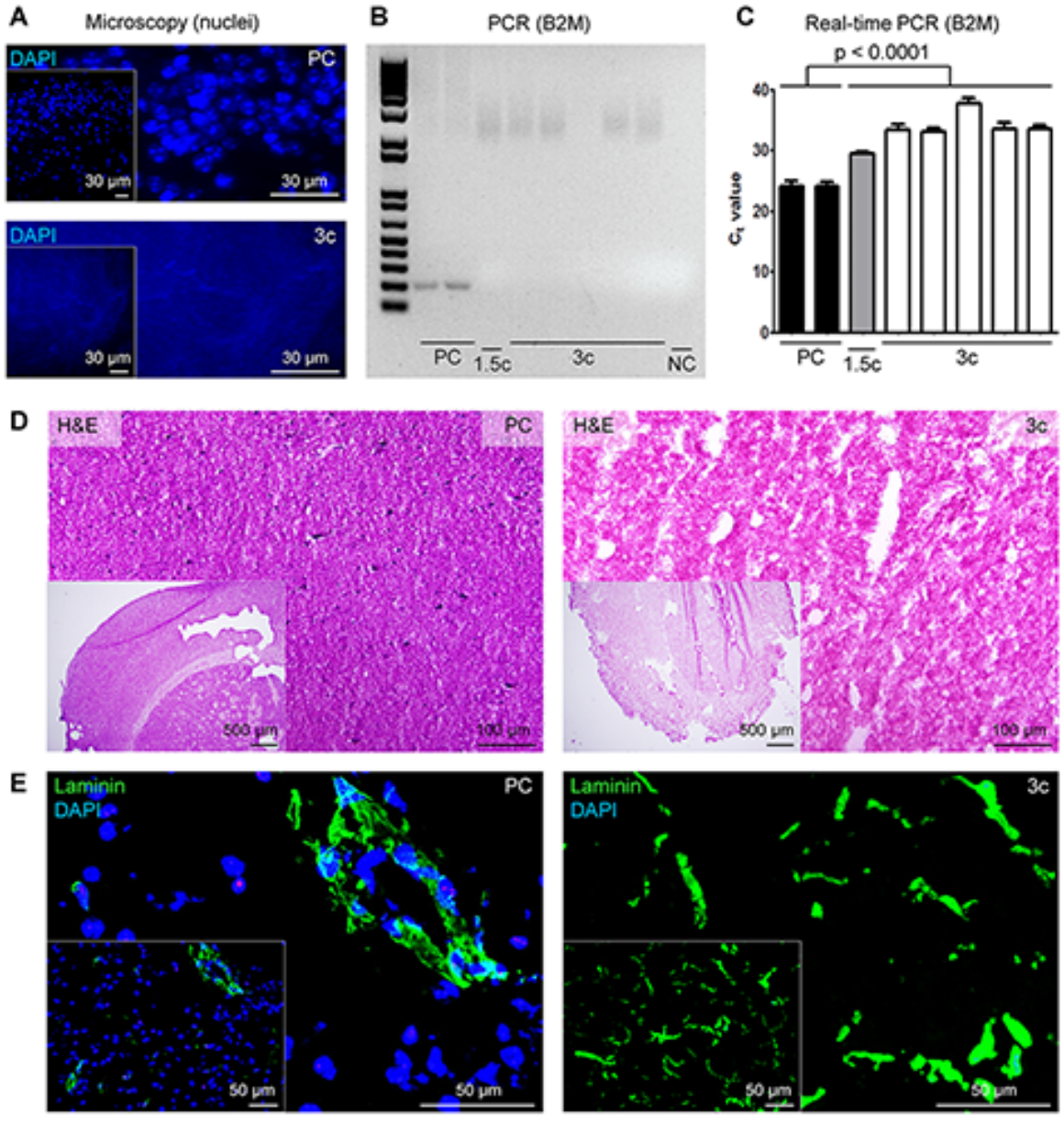
A
Microscopy (nuclei)
DAPI
PC
30 µm
30 µm
DAPI
3c
30 µm
30 µm
B
PCR (B2M)
PC
1.5c
3c
NC
C
Real-time PCR (B2M)
p < 0.0001
C_t value
40
30
20
10
0
PC
1.5c
3c
D
H&E
PC
500 µm
100 µm
H&E
3c
500 µm
100 µm
E
Laminin
DAPI
PC
50 µm
50 µm
Laminin
DAPI
3c
50 µm
50 µm

FIGURE 3

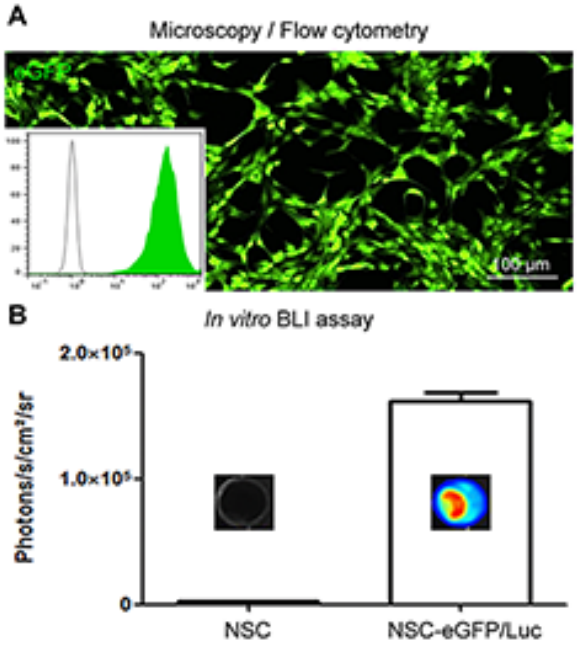
A
Microscopy / Flow cytometry
eGFP
100 µm
B
In vitro BLI assay
2.0×10⁵
1.0×10⁵
0
Photons/s/cm²/sr
NSC
NSC-eGFP/Luc

FIGURE 4

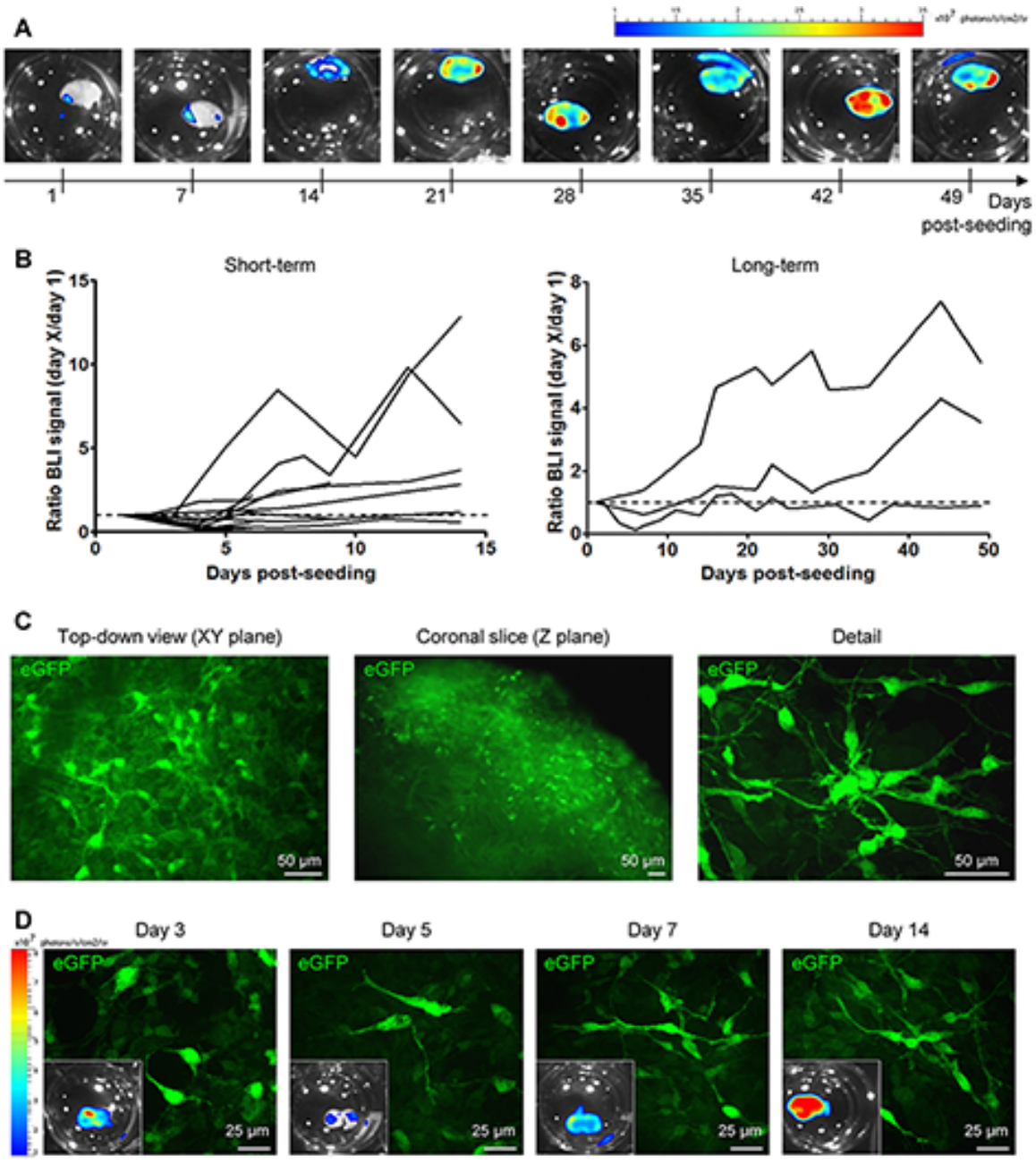
A
1
7
14
21
28
35
42
49
Days post-seeding
B
Short-term
Long-term
Ratio BLI signal (day X/day 1)
Days post-seeding
C
Top-down view (XY plane)
Coronal slice (Z plane)
Detail
eGFP
50 µm
D
Day 3
Day 5
Day 7
Day 14
25 µm

FIGURE 5

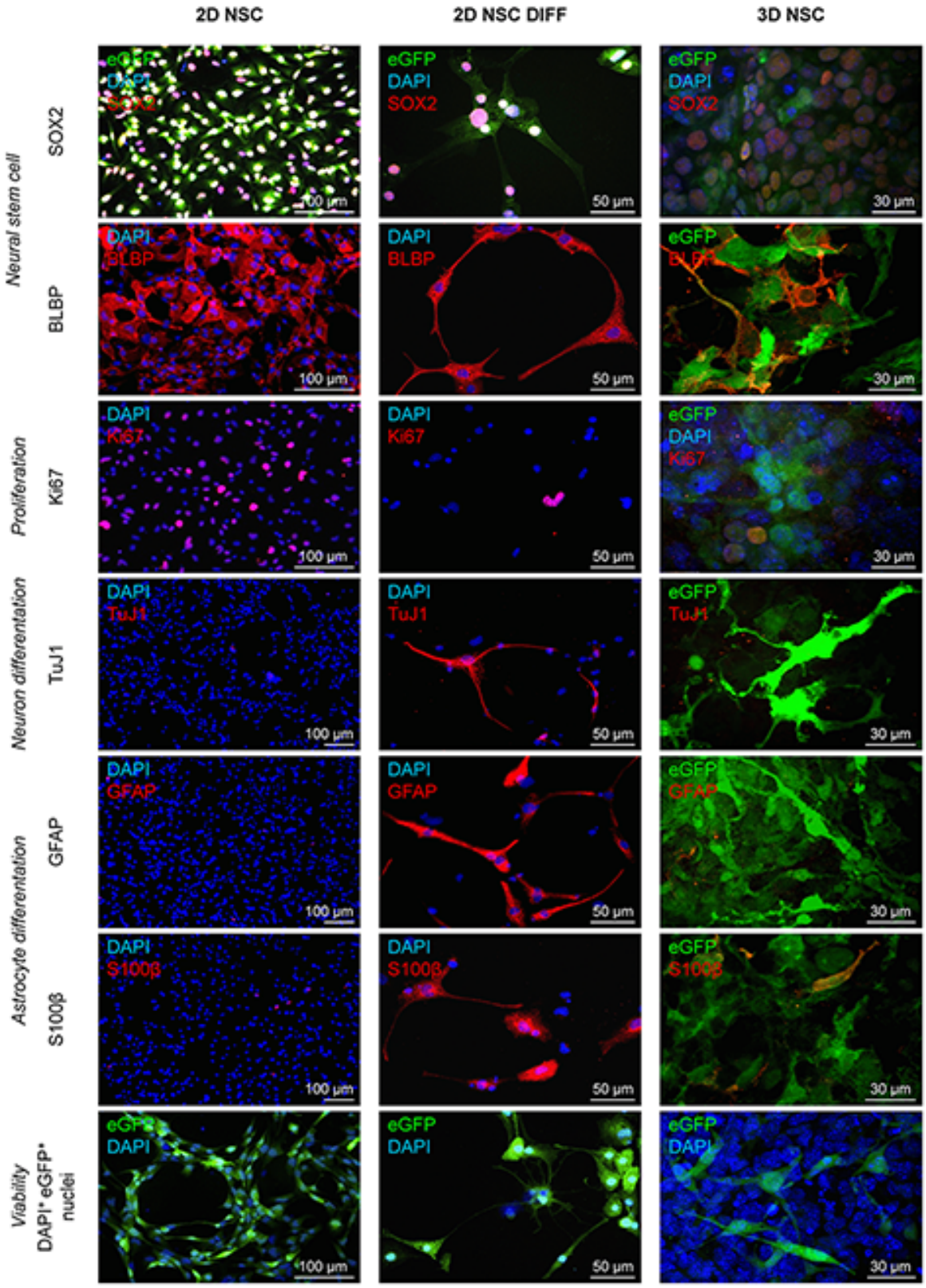
2D NSC
2D NSC DIFF
3D NSC
Neural stem cell
SOX2
BLBP
Proliferation
Ki67
Neuron differentiation
TuJ1
Astrocyte differentiation
GFAP
S100β
Viability
DAPI+ eGFP+ nuclei
eGFP
DAPI
SOX2
BLBP
Ki67
TuJ1
GFAP
S100β
100 µm
50 µm
30 µm

FIGURE 6

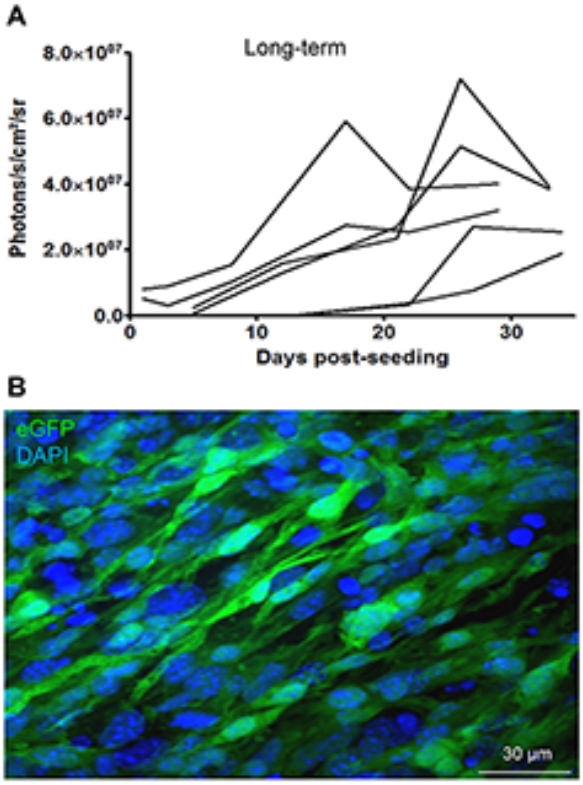
A
Long-term
8.0×10⁰⁷
6.0×10⁰⁷
4.0×10⁰⁷
2.0×10⁰⁷
0.0
Photons/s/cm²/sr
0
10
20
30
Days post-seeding
B
eGFP
DAPI
30 µm

FIGURE S1

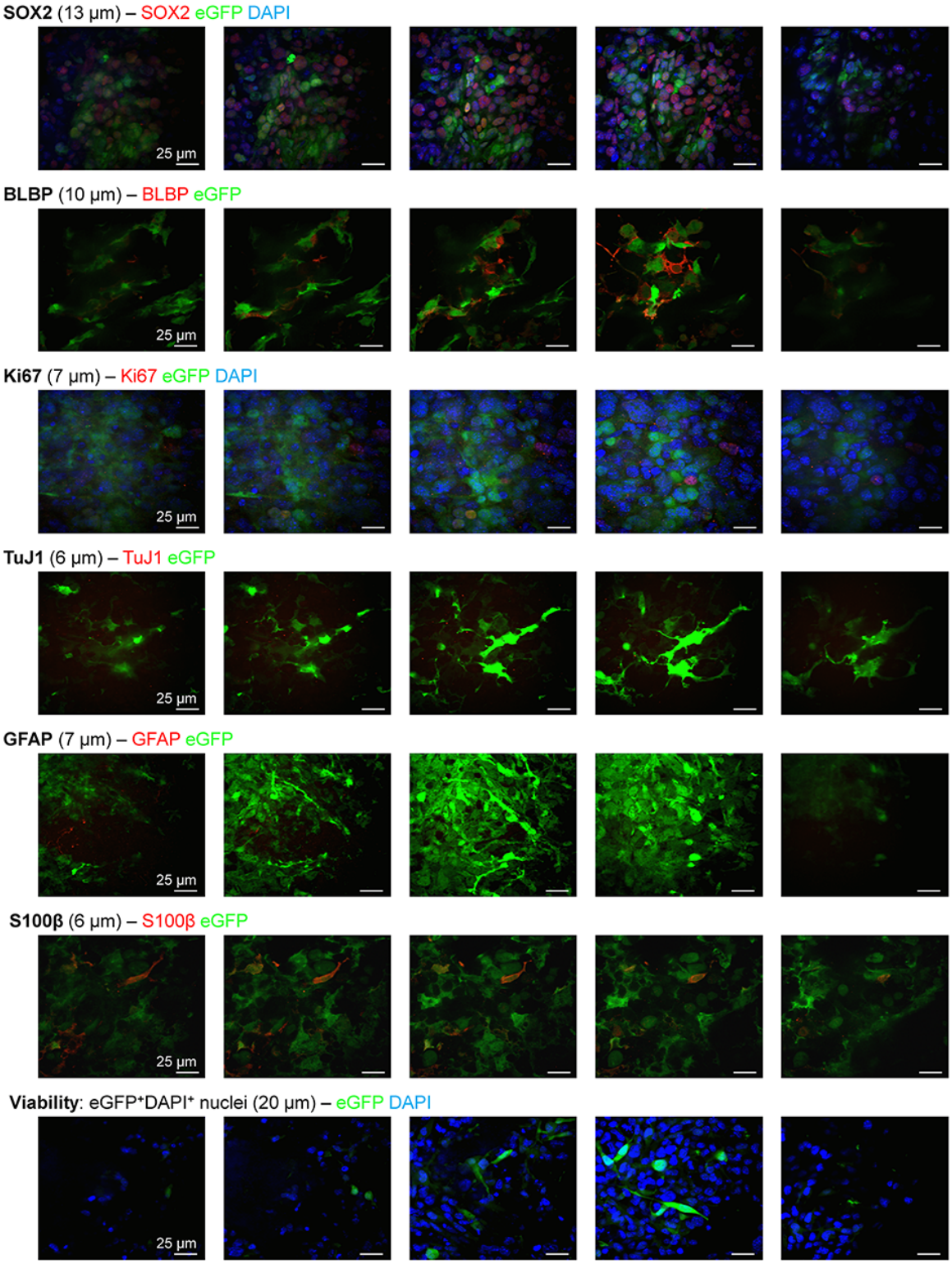
SOX2 (13 µm) – SOX2 eGFP DAPI
25 µm
BLBP (10 µm) – BLBP eGFP
25 µm
Ki67 (7 µm) – Ki67 eGFP DAPI
25 µm
TuJ1 (6 µm) – TuJ1 eGFP
25 µm
GFAP (7 µm) – GFAP eGFP
25 µm
S100β (6 µm) – S100β eGFP
25 µm
Viability: eGFP⁺DAPI⁺ nuclei (20 µm) – eGFP DAPI
25 µm

FIGURE S2